Acetylcholine modulates cerebellar granule cell spiking by regulating the balance of synaptic excitation and inhibition

Abbreviated title: Cholinergic modulation of cerebellar circuits

Taylor R. Fore, Nathan Taylor, Nicolas Brunel, and Court Hull

Department of Neurobiology, Duke University Medical School, Durham, 27710 United States

Correspondence:
Dr. Court Hull
Email: Hull@neuro.duke.edu
Phone: 919-613-0927

Number of Pages: 34
Number of Figures: 9
Number of Words:
Abstract: 243
Introduction: 560
Discussion: 1249

Conflict of Interest Statement:
The authors declare no competing financial interests

Acknowledgements:
This work was supported by grants from the NIH NINDS (5R01NS096289-02), the NSF (DGF1106401) the Sloan Foundation, and the Whitehall Foundation. We thank Dr. Lindsey Glickfeld and members of the Hull and Glickfeld labs for input and technical assistance throughout the project.

Abstract

Sensorimotor integration in the cerebellum is essential for refining motor output, and the first stage of this processing occurs in the granule cell layer. Recent evidence suggests that granule cell layer synaptic integration can be contextually modified, though the circuit mechanisms that could mediate such modulation remain largely unknown. Here we investigate the role of Acetylcholine (ACh) in regulating granule cell layer synaptic integration. We find that Golgi cells, interneurons that provide the sole source of inhibition to the granule cell layer, express both nicotinic and muscarinic cholinergic receptors. While acute ACh application can modestly depolarize some Golgi cells, the net effect of longer, optogenetically induced ACh release is to strongly hyperpolarize Golgi cells. Golgi cell hyperpolarization by ACh leads to a significant reduction in both tonic and evoked granule cell synaptic inhibition. ACh also reduces glutamate release from mossy fibers by acting on presynaptic muscarinic receptors. Surprisingly, despite these consistent effects on Golgi cells and mossy fibers, ACh can either increase or decrease the spike probability of granule cells as measured by non-invasive cell attached recordings. By constructing an integrate and fire model of granule cell layer population activity, we find that the direction of spike rate modulation can be accounted for predominately by the initial balance of excitation and inhibition onto individual granule cells. Together, these experiments demonstrate that ACh can modulate population-level granule cell responses by altering the ratios of excitation and inhibition at the first stage of cerebellar processing.

Significance Statement

The cerebellum plays a key role in motor control and motor learning. While it is known that behavioral context can modify motor learning, the circuit basis of such modulation has remained unclear. Here we find that a key neuromodulator, Acetylcholine (ACh), can alter the balance of excitation and inhibition at the first stage of cerebellar processing. These results suggest that

ACh could play a key role in altering cerebellar learning by modifying how sensorimotor input is represented at the input layer of the cerebellum.

Introduction

To coordinate movements and learn sensorimotor associations, the cerebellum must integrate signals across a variety of modalities and timescales (Giovannucci et al., 2017; Ito, 2006, 2012; Mauk and Buonomano, 2004; Wagner et al., 2017). These signals are conveyed to the cerebellum via mossy fiber projections that form excitatory connections onto a much larger network of granule cells. The divergence from mossy fibers to granule cells has long been hypothesized to enable expansion recoding that enhances pattern separation and increases the encoding capacity of the network (Albus, 1971; Cayco-Gajic et al., 2017; Gilmer and Person, 2017; Marr, 1969).

While classical models of granule cell layer function posit rigid integration rules dictated by the anatomical pattern of mossy fiber to granule cell connectivity, recent studies have demonstrated that the granule cell layer can be contextually modified during behavior. Specifically, granule cell responses to certain sensory modalities can be suppressed during locomotion (Ozden et al., 2012). Moreover, associative learning can be enhanced during locomotion via circuit modulation thought to occur in the granule cell layer (Albergaria et al., 2018). Such contextual modification of granule cell responses may allow for both the enhancement of behaviorally relevant stimuli that should be learned, as well as suppression of information that should not be learned. However, the cellular mechanisms that allow such context-dependent regulation are largely unknown.

Throughout the brain, neuromodulators play a key role in contextual circuit regulation (Froemke et al., 2013; Kuchibhotla et al., 2017; Letzkus et al., 2011). In the cerebellum, there are prominent ACh projections that terminate in the granule cell layer (Jaarsma et al., 1997). Moreover, immunohistochemical studies have shown both nicotinic and muscarinic receptors in

86 the cerebellar cortex (Dominguez de Toro et al., 1997; Dominguez del Toro et al., 1994;
87 Nakayama et al., 1997; Neustadt et al., 1988; Turner and Kellar, 2005). These anatomical
88 observations suggest that ACh could be a key regulator of cerebellar processing and cerebellar-
89 dependent behaviors. Indeed, behavioral studies have demonstrated cholinergic enhancement
90 of the OKR and VOR reflexes (Prestori et al., 2013; Tan and Collewijn, 1991, 1992).

91 To test how acetylcholine acts to modulate granule cell layer processing and synaptic
92 integration, we have investigated both cell autonomous and circuit level effects of ACh by
93 recording from granule cell layer neurons in an acute, in-vitro brain slice preparation. We find
94 that ACh predominantly leads to a prolonged suppression of Golgi cell activity via muscarinic
95 receptor activation, in turn reducing both tonic and evoked synaptic inhibition onto granule cells.
96 In addition, activation of presynaptic muscarinic receptors on mossy fibers leads to a reduction in
97 granule cell excitation. Together, the coincident reduction in excitation and inhibition increases
98 spike probability in some granule cells, while reducing spike probability in others. A population
99 level integrate and fire model of granule cell layer synaptic processing reveals that the direction
100 of modulation depends on the relative balance of excitation and inhibition of individual granule
101 cells. Specifically, we find that the activity of granule cells with the most inhibition is preferentially
102 enhanced by ACh, whereas the activity of granule cells with little inhibition is largely suppressed.
103 Thus, these data suggest that ACh can act to enhance the reliability of granule cells that are
104 significantly inhibited in response to specific mossy fiber input. Such modulation would be well-
105 suited to enhance the responses of granule cells that receive stimulus specific inhibition without
106 expanding the overall population response.

107

108 **Materials and Methods**

109 *Acute Slices and Recordings:*

110 Acute sagittal slices (250 μm) were prepared from the cerebellar vermis of Sprague Dawley rats
111 (20–25 days old, males, Charles River) and ChAT-IRES-Cre mice (B6;129S6-*Chat*$^{tm2(cre)Lowl}$/J,

112 Jackson Labs, P40-60, males and females). Slices were cut in an ice-cold potassium cutting
113 solution (Dugue et al., 2005) consisting of (in mM): 130 K-gluconate, 15 KCl, 0.05 EGTA, 20
114 HEPES, 25 glucose (pH 7.4, 320 mmol/kg), and were transferred to an incubation chamber
115 containing artificial CSF comprised of (in mM): 125 NaCl, 26 $NaHCO_3$, 1.25 NaH_2PO_4, 2.5 KCl, 2
116 $CaCl_2$, 1 $MgCl_2$, and 25 glucose (pH 7.3, 320 mmol/kg). A NMDA antagonist, *R*-CPP (2.5 μM,
117 Tocris), was added to the potassium cutting solution to enhance cell survival. Slices were
118 incubated at 32° C for 20 minutes, and then kept at room temperature for up to 7 hours. All
119 solutions were saturated with 95% O_2 and 5% CO_2. All procedures were performed according to
120 guidelines approved by the Duke University Institutional Animal Care and Use Committee.
121
122 Visually guided (SliceScope Pro 2000 with Dodt-gradient contrast and water-immersion 60x
123 objective, Scientifica) whole-cell recordings were obtained using a Multiclamp 700B (Axon
124 Instruments) with thick-walled borosilicate glass patch pipettes (Granule cells, whole cell: 5-7 MΩ,
125 Granule cells, cell attached: 10-14 MΩ, Golgi cells: 2-4 MΩ; 1.5 mm OD, 0.84 mm ID, World
126 Precision Instruments). Electrophysiological recordings were digitized at 20 kHz (Digidata 1440A,
127 Axon Instruments), filtered at 10 kHz, and performed at 32-33 °C. Glass monopolar electrodes (1
128 MΩ) filled with aCSF, in conjunction with a stimulus isolation unit (ISO-Flex, A.M.P.I.), were used
129 for extracellular stimulation of the mossy fiber tract. For cell-attached recordings, only cells with
130 an initial spike probability in control conditions between approximately 20% and 60% were
131 recorded to allow for increases or decreases in spike rate during pharmacological manipulations.
132
133 Spontaneous and evoked IPSCs were recorded at the EPSC reversal potential (+10 mV). Evoked
134 excitatory postsynaptic currents (eEPSC) were recorded at a holding potential of -70 mV and -60
135 mV for granule cells and Golgi cells, respectively. Voltage-clamp recordings of IPSCs and EPSCs
136 were collected using a cesium-based internal solution containing (in mM): 140 Cs-gluconate, 15
137 HEPES, 0.5 EGTA, 2 TEA-Cl, 2 MgATP, 0.3 NaGTP, 10 Phosphocreatine-$Tris_2$, 2 QX-314 Cl, pH

138 was adjusted to 7.2 with CsOH, resulting in a final osmolality of 316 mmol/kg. Current-clamp and
139 voltage-clamp recordings of Golgi cells were performed using a potassium-based internal solution
140 containing (in mM): 150 K-gluconate, 3 KCl, 10 HEPES, 0.5 EGTA, 3 MgATP, 0.5 NaGTP, 5
141 Phosphocreatine-$Tris_2$, 5 Phosphocreatine-Na_2, pH was adjusted 7.2 with KOH, osmolality: 315
142 mmol/kg. Membrane potentials were not corrected for the liquid junction potential. Series
143 resistance was monitored during voltage-clamp recordings with a 5 mV hyperpolarizing pulse,
144 and only recordings that remained stable over the period of data collection were used. All drugs
145 were purchased from Abcam or Tocris.
146
147 *Virus Injections and Optogenetic Experiments:*
148 Expression of the optogenetic actuator Chronos in ChAT+ cerebellar projection neurons was
149 achieved using retro-orbital injection (2-10 μL)(Yardeni et al., 2011) of AAV-PHP.eb-Syn-FLEX-
150 rc[Chronos-tdTomato] into ChAT-IRES-Cre mice (B6;129S6-*Chat*$^{tm2(cre)Low/}$/J, Jackson Labs)
151 at P0-P2. Recordings with optogenetic stimulation were subsequently performed between P40-
152 P60. Labeled axons in these experiments were observed throughout the cerebellar vermis,
153 including both thin fibers and mossy fiber-like axons. Mossy fiber-like axons were most dense in
154 lobules VIII-X. Experiments were performed in any vermis lobule where labeling was evident as
155 visualized by Td-Tomato expression during experiments. Optogenetic stimulation was performed
156 using full-field illumination (50 Hz, 2-3 sec, 10-20 mW) with a 450 nm laser (Optoengine, MGL-III-
157 450).
158
159 *Data Analysis:*
160 IPSCs and EPSCs were analyzed using Clampfit, Igor Pro, and Mini Analysis software (v6.0.3,
161 Synaptosoft Inc.) using a 3 kHz low pass Butterworth filter. Detection thresholds for single trial
162 responses were set to 5x (IPSCs) or 2.5x (EPSCs) greater than the baseline RMS noise level.
163 Synaptic potency was measured as the amplitude on all trials where EPSCs or IPSCs were

164 successfully evoked, excluding failures. Mossy fiber paired-pulse ratios were determined using
165 an inter-stimulus interval (IS) of 40 ms and measured from an average waveform across 30
166 consecutive trials. For voltage-clamp recordings of nicotinic and muscarinic currents, peak current
167 amplitudes were measured from the subtracted average current for each cell. For cell attached
168 recordings, spike probabilities were calculated in 1 ms bins, and normalized to the maximum spike
169 probability on a per cell basis. Spike rates were calculated across all three stimuli in a 45 ms
170 window and normalized to control. Data are reported as mean ± SEM (unless otherwise noted),
171 and statistical analysis was carried out using custom R package (available at
172 github.com/trfore/MAtools) and Clampfit (Molecular Devices). Data was tested for
173 homoscedasticity using Brown-Forsythe test and for normality via quantile-quantile plots. For
174 heteroscedastic data, we applied a repeated measures ANOVA with Dunnett's post hoc test;
175 additionally, sphericity was not assumed and a Greenhouse-Geisser correction was applied.
176 Alternatively, a one-way ANOVA with Tukey post hoc was used. Significant differences are
177 denoted as follows: *** = $p < 0.001$, ** = $p < 0.01$, and * = $p < 0.05$.
178
179 *Modelling:*
180 The granular layer model was simulated with the Brian simulator (http://briansimulator.org). The
181 structure of the network was adapted from Solinas et al. (Solinas et al., 2010), which aims to
182 recreate a functionally relevant cube of the cerebellar granular layer with 100 μm edge length.
183 The model comprised 315 mossy fibers, 4096 granule cells, and 27 Golgi cells. Probabilistic
184 synapses were formed using the convergence ratios in Table 1, with the probability of a particular
185 presynaptic neuron making a connection with a particular postsynaptic neuron defined as p =
186 (Conv. ratio) / (Total no. presynaptic neurons). There were no spatial constraints on synapse
187 formation.
188
189 Table 1.

	Number	*Conv. ratio*	*Synapse prob.*
mf	315		
GrC	4096		
GoC	27		
mf → GrC		4:1	0.0127
mf → GoC		10:1	0.0317
GoC → GrC		4:1	0.1481

Granule and Golgi cells were modeled as conductance-based leaky integrate-and-fire neurons with sub-threshold membrane dynamics governed by:

$$C_m \frac{dv}{dt} = g_l(E_l - v) + (g_e + g_n)(E_e - v) + (g_i + g_t)(E_i - v)$$

for granule cells, and

$$C_m \frac{dv}{dt} = g_l(E_l - v) + (g_e + g_n)(E_e - v)$$

for Golgi cells, where C_m is the membrane capacitance; v is the membrane potential; E_l, E_e, and E_i are leak, excitatory, and inhibitory reversal potentials; g_l, g_e, and g_i are leak, excitatory, and (phasic) inhibitory conductances; g_t is the (fixed) tonic inhibitory conductance in granule cells; and g_n is a stochastically fluctuating excitatory conductance described by an Ornstein-Uhlenbeck process,

$$\tau_n \frac{dg_n}{dt} = -g_n + \sigma_n \sqrt{\tau_n} \xi(t),$$

where $\xi(t)$ is a white noise with unit variance density. Table 2 lists the fixed parameters for each cell type in control conditions. In control, Golgi cells fired spontaneously on average between 1 and 6 Hz. This spontaneous activity was achieved by setting the Golgi cell leak reversal E_l near spike threshold and allowing the stochastic excitatory current to occasionally drive the cell above

threshold. Application of GABAzine was simulated by eliminating both tonic and phasic inhibition onto granule cells, without changing Golgi cell excitability. Tonic release of acetylcholine was simulated by suppressing Golgi cell activity (viz., by setting the leak reversal back to the resting membrane potential) and reducing the magnitude of mossy fiber excitation onto both granule and Golgi cells by 54.79% and 54.22% of their control values, respectively, as per experimental results. Tonic inhibition was reduced differentially across granule cells by a fraction drawn from a Gamma distribution with mean 0.6 and standard deviation 0.07.

Table 2.

	v_r	v_{th}	C_m	g_l	g_t	E_l	E_e	E_i	σ_n	τ_n	τ_e	τ_i
	(mV)		*(pF)*	*(nS)*			*(mV)*		*(nS)*		*(ms)*	
GrC	-75	-55	3.1	0.2	1	-75	0	-75	0.05	20	12	20
GoC	-55	-50	60	3	0	-51	0	-75	0.1	20	12	-

Three conditions (control, GABAzine, muscarine) were each simulated for 100 trials, each trial running for two seconds. Trials were simulated for one second without mossy fiber input to allow for decorrelation of GrC and GoC populations. Mossy fiber stimulation was modeled as three spikes delivered to a random selection of 32 mossy fibers at 1.01, 1.02, and 1.03 s. The same 32 mossy fibers were stimulated across all trials of an individual simulation. Each mossy fiber was assigned a mean synaptic weight from a gamma distribution with a mean and standard deviation of 0.1 nS. Following a presynaptic mossy fiber spike, excitatory postsynaptic conductance g_e in both granule and Golgi cells was instantaneously increased by a synaptic weight drawn from a gamma distribution with mean and standard deviation equal to that mossy fiber's assigned mean. A presynaptic Golgi cell spike elicited a fixed instantaneous jump in the inhibitory conductance g_i on the postsynaptic granule cell with a 2 ms delay. Synaptic conductances decayed following the equations:

234 $$\tau_e \frac{dg_e}{dt} = -g_e$$

235 and

236 $$\tau_i \frac{dg_i}{dt} = -g_i,$$

237

238 where τ_e and τ_i are decay time constants specific to excitation and inhibition in each cell type.
239 Upon reaching threshold v_{th}, the membrane potential was immediately reset to its resting rate v_r,
240 and held there for an absolute refractory period of 2 and 10 ms for granule and Golgi cells,
241 respectively.

242

243 Excitatory and inhibitory conductance traces were recorded for each granule cell during the
244 simulation, as well as spike times. Spike probabilities were calculated in 1 ms bins over the 100
245 trials, and normalized to the peak spike probability on a per cell basis. Only granule cells with
246 active mossy fiber input and a nonzero spike probability ratio in control were considered for
247 subsequent analysis. To match with experimental criteria, we further selected for those cells
248 whose peak spike probability to the second stimulus did not exceed 0.6, and whose peak spike
249 probability to the third stimulus did not exceed that to the second. Cells categorized as 'increasing'
250 spike probability in muscarine had a mean normalized spike probability greater than 1, while
251 'decreasing' cells had a mean normalized spike probability less than 1. Average conductance was
252 calculated by integrating each conductance trace over a 60 ms period starting 10 ms before the
253 first stimulus and ending 30 ms after the final stimulus, then dividing by that interval.

254

255 **Results**

256 **Cholinergic modulation of Golgi Cells**

257 Anatomical studies have reported nicotinic and muscarinic receptors in the cerebellar
258 cortex (Jaarsma et al., 1997). Additionally, functional studies have found α7-nAChRs (Prestori et

259 al., 2013), α4β2-nAChRs, and M3-mAChRs on granule cells; however, α4β2-nAChRs are
260 reportedly developmentally down-regulated (Didier et al., 1995) and the M3-mAChRs are
261 expressed in ~15% of granule cells in lobules IX-X (Takayasu et al., 2003). To test for functional
262 cholinergic receptors in the adult cerebellar granule cell layer, we performed whole-cell recordings
263 from Golgi and granule cells in the presence of synaptic receptor antagonists (NBQX 5 μM, R-
264 CPP 2.5 μM, and SR95531 5 μM), and focally applied acetylcholine (ACh 500 μM, 200 ms) via a
265 second pipette positioned in close proximity (~5-20 μm) to the recorded somata.

266 Golgi cells are the primary inhibitory interneuron in the granule cell layer, providing the
267 main source of synaptic inhibition to granule cells. Because Golgi cells fire spontaneously
268 between 1 to 20 Hz (Forti et al., 2006) , we first tested for acetylcholine-mediated regulation of
269 their spontaneous firing (**Figure 1A**). Brief application of ACh caused a transient increase in the
270 firing rates of 7 of 10 recorded Golgi cells (5.3 ± 1.2 fold, n = 7 of 10, **Figure 1B, C, D**). However,
271 in all recorded Golgi cells, there was a longer lasting suppression of firing (0.13 ± 0.06 fold, n =
272 10). To test what synaptic currents were responsible for these changes in spontaneous firing rate,
273 we recorded in voltage-clamp configuration from a subset of the same cells. Focal application of
274 ACh revealed a prolonged outward current that was blocked by the selective type II muscarinic
275 receptor antagonist AF-DX 116 (1 μM)(16.1 ± 2.6 pA, n = 7, **Figure 1E,F**), as well as a transient
276 inward current that was blocked by the non-selective nicotinic receptor antagonist MMA (10 μM)
277 (40.3 ± 11.4 pA, n = 7, **Figure 1E,F**). In contrast, granule cell recordings revealed no change in
278 membrane potential in response to ACh application in current-clamp, and no nicotinic nor
279 muscarinic receptor-activated currents in voltage-clamp (n = 24, **Figure 1 G-J**).

280 Focal application of ACh onto Golgi cells suggests the possibility of long-term suppression
281 during periods of ongoing acetylcholine release when nicotinic receptors are desensitized. To test
282 this, we simulated tonic release of acetylcholine by bath application of muscarine (10 μM) in the
283 presence of TTX (0.5 μM) to block spontaneous pacemaking (**Figure 2A**). In these experiments,

284 muscarine produced a prolonged hyperpolarization that lasted the duration of the agonist
285 application, and was abolished in the presence of the non-selective muscarinic receptor
286 antagonist atropine (5 μM). To test whether such long-term modulation could be achieved by
287 endogenous release of ACh, we expressed the optogenetic actuator chronos in cerebellar
288 projecting cholinergic neurons (methods), and stimulated labeled axons in cerebellar vermis using
289 2-3 second pulse trains (50 Hz) of blue light (**Figure 2 B-E**). This stimulation protocol produced
290 a modest depolarizing current during the stimulation, but predominantly resulted in a long-lasting,
291 atropine sensitive outward current that emerged after the stimulus and persisted for 10s of
292 seconds (**Figure 2D,E**). Overall, these finding suggest that ongoing bouts of granule cell layer
293 ACh release can activate M2 muscarinic receptors on Golgi cells that produces a long-lasting, net
294 suppression of these interneurons.
295
296 **Cholinergic regulation of granule cell tonic inhibition**
297 Golgi cells are the main source of granule cell synaptic inhibition (Eccles et al., 1966;
298 Farrant and Brickley, 2003; Kanichay and Silver, 2008). Specifically, GABA released from Golgi
299 cells activates two types of granule cell $GABA_A$ receptors to regulate granule cell excitability
300 (Brickley et al., 1996; Crowley et al., 2009; Duguid et al., 2015; Duguid et al., 2012). Based on
301 our measurements of muscarinic receptor-mediated Golgi cell suppression, we next tested for
302 changes in tonic granule cell synaptic inhibition during simulated bulk release of acetylcholine
303 using bath application of muscarine (**Figure 3**). Bath application of muscarine resulted in a
304 significant decrease in both spontaneous IPSC (sIPSC) frequency (83.7 ± 2.9% decrease, control:
305 4.5 ± 0.8 Hz, muscarine: 0.8 ± 0.3 Hz, n=11, P<0.0001, **Figure 3B**) and a tonic inhibitory current
306 mediated by non-desensitizing $GABA_A$ receptors (54.3 ± 3.3% decrease, control: 8.85 ± 1.08 pA,
307 muscarine: 4.1 ± 0.7 pA, P<0.0001, **Figure 3C**). These effects were reversed by atropine (sIPSC
308 frequency: 4.9 ± 0.9 Hz, holding current: 7.5 ± 1.0 pA, **Figure 3B-D**), suggesting that M2 receptor-

309 mediated suppression of Golgi cell firing can significantly reduce tonic granule cell synaptic
310 inhibition.
311
312 **Activation of Golgi Cell M2 receptors induces spike rate plasticity**
313 In a subgroup of granule cells, sIPSC frequency increased following bath application of
314 muscarine (1.7 ± 0.2 of control, n=5 of 11, P = 0.015, **Figure 3D**). These data suggest an increase
315 in spontaneous Golgi cell firing rates following muscarine application. Previous work has
316 demonstrated that Golgi cell pacemaking can undergo a form of long-term firing rate potentiation
317 following extended membrane hyperpolarization (Hull et al., 2013). To test whether activation of
318 M2 receptors could provide an endogenous mechanism for inducing this plasticity, we performed
319 whole-cell current clamp recordings from Golgi cells in the presence of synaptic receptor
320 antagonists (NBQX 5 μM, CPP 2.5 μM, SR95531 5 μM) while simulating bulk acetylcholine
321 release via bath application of muscarine (10 μM). Muscarine reliably suppressed GoC spiking
322 throughout the application period (baseline: 4.2 ± 0.6 Hz; musc: 0.5 ± 0.3 Hz; **Figure 4A**).
323 Following subsequent atropine application, Golgi cell firing resumed at rates that were, on
324 average, higher than in control (5.5 ± 0.7 Hz, **Figure 4A**). In agreement with previous work (Hull
325 et al., 2013), this firing rate potentiation was preferential to Golgi cells with low baseline firing rates
326 (FRP; <5Hz: 1.6 ± 0.2 norm, n=13; >5Hz: 1.0 ± 0.1 norm, n=4; **Figure 4B-D**). These results
327 suggest that acetylcholine can act as an endogenous mechanism for inducing Golgi cell firing rate
328 potentiation by activating M2 muscarinic receptors. Moreover, the diversity of plasticity across
329 Golgi cells with different initial firing rates was in agreement with the diversity of changes in sIPSC
330 rates in granule cells following muscarine application (**Figure 3D**).
331
332 **Cholinergic regulation of evoked granule cell inhibition**
333 Golgi cells also provide evoked feed-forward inhibition in response to mossy fiber
334 activation that serves to regulate excitability during cerebellar input (Duguid et al., 2015; Kanichay

335 and Silver, 2008). To test how evoked granule cell inhibition is regulated by ongoing cholinergic
336 modulation, we electrically stimulated the mossy fibers during bath application of muscarine.
337 Mossy fiber stimulation reliably evoked IPSCs (control: 51.8 ± 8.4 pA, 12.8 ± 5.8% failure rate, n
338 = 5, **Figure 5**). In the presence of muscarine, evoked IPSC amplitudes decreased significantly
339 (98.2 ± 0.8% decrease, 0.6 ± 0.4 pA, P<0.0001, **Figure 5 B-D**), and the failure rate increased
340 significantly (98.4 ± 0.8% failure rate, P=0.0004, **Figure 5E**). Atropine reversed these effects on
341 the evoked IPSC amplitude (11.0 ± 15.7%, 53.0 ± 9.9 pA, **Figure 5D**) and failure rate (19.3 ±
342 7.1% failure rate, **Figure 5E**). Importantly, evoked IPSCs were di-synaptically evoked, as
343 glutamatergic antagonists (NQBX 5 μM, CPP 2.5 μM) abolished all evoked IPSCs (100 ± 0%
344 failure rate, **Figure 5E**). The muscarine-induced reduction in evoked IPSC amplitude and
345 increase in failure rates are consistent with our finding of muscarinic receptor-mediated Golgi cell
346 hyperpolarization. However, because these experiments rely on stimulated mossy fiber input, it
347 is also possible that a muscarinic receptor-mediated reduction in presynaptic mossy fiber input to
348 Golgi cells could also contribute to the observed reduction in evoked IPSCs.
349

350 **Presynaptic Muscarinic Receptors reduce Mossy Fiber input to the granule cell layer**

351 To test whether long-term cholinergic release could also regulate the efficacy of
352 glutamatergic mossy fiber inputs, we next tested how bath application of muscarine regulates
353 EPSCs onto both Golgi cells and granule cells. We first tested for the presence of muscarinic
354 receptors at mossy fiber to Golgi cell synapses (**Figure 6**). In response to mossy fiber stimulation,
355 muscarine significantly decreased the amplitude of evoked EPSCs onto Golgi cells (50.7 ± 11.7%
356 , control: 127.0 ± 16.6 pA, muscarine: 61.4 ± 22.1 pA, atropine: 120.2 ± 18.7 pA, n=10, P=0.0028,
357 **Figure 6B-D**) and increased the failure rate (control: 2.2 ± 1.0%, muscarine: 29.6 ± 8.5%,
358 atropine: 2.2 ± 0.6%, P<0.0001, **Figure 6E**). Notably, we did not observe a significant increase
359 in paired-pulse ratio in muscarine, as would be expected if muscarine acts presynaptically to
360 reduce release probability (**Figure 6G**). However, mossy fibers also express $GABA_B$ receptors,

361 and muscarine silences Golgi cell spiking to reduce ongoing GABA release. Thus, muscarine
362 should also reduce presynaptic $GABA_B$ receptor activation, and this effect could serve to produce
363 a competing increase release probability. In the presence of the $GABA_B$ receptor antagonist CPG
364 54626 (1 μM), however, muscarine produced only a modest trend toward larger paired-pulse
365 ratios (control PPR = 0.9 ± 0.0, muscarine PPR = 1.0 ± 0.1, p = 0.7, **Figure 6H**). We note,
366 however, that the strong reduction in EPSC amplitude and multiple EPSC failures in muscarine
367 add considerable variability to PPR measurements in this condition.

368 To test whether presynaptic regulation of mossy fiber input is selective to Golgi cell
369 synapses, we next measured evoked EPSCs onto granule cells during bath application of
370 muscarine (**Figure 7**). Again, we found a significant decrease in mossy fiber-evoked EPSCs in
371 muscarine, along with a significant increase in failure rate (52.8 ± 9.60% EPSC decrease, control:
372 68.6 ± 10.7 pA, muscarine: 32.4 ± 8.8 pA, n = 10, control failure rate: 0.3 ± 0.3%, muscarine: 26.3
373 ± 7.5%, **Figure 7B-F**). These effects were reversed in atropine (11.8 ± 4.4%, amplitude: 64.0 ±
374 11.4 pA, failure rate: 1.3 ± 0.7%, **Figure 7B-F**). As with Golgi cell synapses, muscarine did not
375 significantly increase the paired-pulse ratio (control: 0.8 ± 0.0 muscarine: 0.9 ± 0.1, atropine: 0.8
376 ± 0.0, P = 0.4889, **Figure 7G**). These data reveal that ongoing ACh release can reduce the
377 efficacy of excitatory glutamatergic mossy fiber input to granule cell layer neurons by activating
378 presynaptic muscarinic receptors.

379

380 **Muscarinic receptor activation produces bi-directional changes in granule cell spike**
381 **probability**

382 Our results show that ACh can act through muscarinic receptors to reduce both incoming
383 excitation and synaptic inhibition in the granule cell layer. To test how these effects combine at
384 the circuit level to regulate granule cell activity, we performed non-invasive cell-attached
385 recordings from granule cells while stimulating mossy fiber input (**Figure 8**). Across 8 recorded
386 granule cells that spiked in response to mossy fiber stimulation (methods), bath application of

387 muscarine significantly altered spike probability (**Figure 8 C-F**). Importantly, however, modulation
388 of granule cell spiking fell into two distinct categories: In 5 of 8 granule cells, we observed an
389 increase in granule cell spike probability and rate in response to muscarine application
390 (muscarine: 1.9 ± 0.3 normalized rate, n = 5, p = 0.0814, **Figure 8C, D**). The remaining 3 granule
391 cells exhibited a large decrease in spike probability and rate following muscarine application
392 (muscarine: 0.2 ± 0.2 S.D. normalized rate, n = 3, p = 0.0612, **Figure 8E, F**). In contrast, blocking
393 all ionotropic GABAergic inhibition (SR95531 5 μM) dramatically increased spike probabilities and
394 rates uniformly across all recorded granule cells (muscarine: 1.2 ± 0.4 normalized, GABAzine: 6.8
395 ± 1.6; ANOVA $F_{1.076,\ 7.53}$ = 14.95, P=0.0049, n = 8, **Figure 8C-G**). Consistent with the fast
396 membrane time constant of granule cells (Fleming and Hull, 2019), however, neither muscarine
397 nor SR95531 altered the timing of the first spikes in response to stimulation (mean ± S.D. stim 1:
398 control = 3.5 ± 1.3 ms, musc = 4.3 ± 2.0 ms; stim 2: control = 2.3 ± 0.8 ms, musc = 2.5 ± 1.4 ms;
399 stim 3: control = 2.5 ± 1.2 ms, musc = 2.8 ± 1.4 ms; n=5; **Figure 8H**). Thus, these data reveal
400 that muscarine can alter granule cell responses by enhancing the reliability and rate of spiking in
401 some granule cells receiving mossy fiber input, and reducing spike probability and rate in others.
402

403 **Network model of granule cell spiking in response to muscarinic neuromodulation**

404 How does muscarine produce this population level, bi-directional change in granule cell
405 spiking? Because it is not possible to record sub-threshold excitation and inhibition across
406 pharmacological conditions in the same granule cells where cell-attached recordings of spiking
407 were performed, we generated a network model of granule cell activity to test what parameters
408 determine whether granule cells will increase or decrease their spike probabilities in response to
409 muscarinic neuromodulation. As muscarine reduces both excitatory and inhibitory inputs to
410 granule cells, we expect intuitively that the net effect on granule cell firing will depend on which
411 reduction is strongest – granule cells in which excitatory inputs are more strongly reduced than

412 inhibitory inputs should decrease their spiking activity, while the opposite should occur in the
413 opposite situation where inhibitory inputs are more reduced.

414 To test this hypothesis, we simulated a granular layer network of 4,096 granule cells and
415 27 Golgi cells, receiving inputs from 315 mossy fibers, with realistic connectivity parameters
416 (methods). In this network simulation, we implemented all the effects of muscarine characterized
417 above, in such a way as to match experimental results (methods). Upon stimulation of a random
418 subset of 32 mossy fibers, granule cell spiking activity was qualitatively similar to the slice
419 preparation. Of the 319 granule cells that spiked in response to mossy fiber stimulation, 85
420 exhibited an increase in spiking activity in the simulated presence of muscarine (peak spike
421 probability in muscarine: 2.53 ± 0.13, normalized to control, **Figure 9 A,C**), while 65 showed
422 decreased spiking activity (peak spike probability in muscarine: 0.33 ± 0.04, normalized to control,
423 **Figure 9 B,C**). The remaining granule cells did not change spike probability, and were excluded
424 from further analysis.

425 We found no significant correlation between the number of active mossy fiber inputs and
426 the change in spike probability in muscarine (Spearman's correlation; $r = 0.03$ $p = 0.66$, **Figure 9**
427 **D**). However, cells exhibiting an increase in spike probability were dominated by inhibition in
428 control conditions (net conductance: -0.51 ± 0.08 nS, **Figure 9 E,G**), whereas cells with
429 decreasing spike probability received relatively less Golgi cell input (net conductance: 0.20 ± 0.07
430 nS, **Figure 9 E,G**). Moreover, there was a preferentially greater reduction in tonic inhibition of
431 cells with increased spiking activity (increasing: 65.5 ± 1% reduction, decreasing: 55.7 ± 1%
432 reduction, Kolmogorov-Smirnov $D = 0.62$, $p < 0.0001$, **Figure 9 F, G**).

433 We tested that our results did not depend on a specific realization of the network
434 connectivity by simulating 30 independent realizations of the connectivity matrix, and patterns of
435 input mossy fiber stimulation. While the relative numbers of cells exhibiting increases and
436 decreases in spike probability were variable across different instantiations of the model, the

437 underlying input profiles distinguishing the two cell categories were comparable (increasing cells
438 had a net inhibitory conductance in control: -0.40 ± 0.03 nS, decreasing cells had a net excitatory
439 conductance in control: 0.26 ± 0.03 nS, not shown). Similarly, we saw consistently larger
440 decreases in the inhibitory tonic current between for cells that increased their spike probability in
441 muscarine (increasing: 64.7 ± 0.2% reduction, decreasing: 57.6 ± 0.2% reduction, not shown).
442 Together, these results indicate that muscarinic neuromodulation preferentially enhances the
443 spike rates of granule cells with larger synaptic inhibition in control conditions.
444
445
446 **Discussion**
447 Here we have shown that acetylcholine activates muscarinic receptors to modulate two of
448 the three main nodes within the granule cell layer of the cerebellar cortex. Specifically, both Golgi
449 cells and mossy fibers express muscarinic receptors that serve to hyperpolarize Golgi cells and
450 decrease mossy fiber release probability respectively. By simulating ongoing release of
451 acetylcholine using bath application of muscarine, we revealed a suppression of Golgi cell spiking
452 that is mediated by M2-type muscarinic receptors. Consistent with this finding, optogenetic
453 stimulation of ChAT+ cerebellar projections produced a long-lasting, net hyperpolarizing current
454 in Golgi cells that greatly outlasted the duration of stimulation. At the circuit level, suppression of
455 Golgi spiking led to a large decrease in synaptic inhibition onto granule cells. In parallel, muscarine
456 also reduced excitatory transmission from mossy fibers by acting on presynaptic muscarinic
457 receptors.
458 Together, by acting on both Golgi cells and mossy fibers, we find that ACh can alter the
459 coordination of excitation and inhibition onto granule cells. Surprisingly, however, these changes
460 in excitation and inhibition produce diverse changes in granule cell spiking at the population level.
461 Specifically, spike probability in some granule cells can be enhanced, while others are largely
462 suppressed. By generating a network model of the granule cell layer, we provide evidence that

463 the direction of spike rate modulation is established by the initial balance of excitation and
464 inhibition onto each cell, as well as the degree to which neuromodulation reduces tonic inhibition.
465 Overall, cells with higher levels of inhibition increased their spike rates in response to
466 neuromodulation, while cells with less inhibition decrease their spike rates. These changes are
467 in stark contrast to the responses observed after removing all inhibition, which dramatically
468 increases spiking of the entire population. Thus, these data suggest that by simultaneously
469 reducing excitation and inhibition, cholinergic neuromodulation can provide a mechanism for
470 enhancing the responses of subsets of granule cells without expanding the overall population
471 response.

472 Under what conditions might ACh act to modulate the granule cell layer in vivo? Previous
473 work suggests that ChAT+ cerebellar projecting neurons originate from diverse sources (Jaarsma
474 et al., 1997). Consistent with our findings, these projections can take the form of mossy fiber-like
475 inputs, or thinner beaded fibers (Jaarsma et al., 1997). Previous studies have shown that ChAT+
476 mossy fiber terminals and beaded fibers are expressed throughout the cerebellar cortex, with
477 lobules IX/X having the densest mossy fiber innervation and lobule IX having the densest beaded
478 fiber innervation (Barmack et al., 1992a; Jaarsma et al., 1996; Ojima et al., 1989). We also
479 observed the densest innervation of ChAT+ mossy fiber-like terminals in these lobules, though
480 ChAT+ terminals were present in all lobules, and we observed optogenetically driven currents in
481 Golgi cells throughout the vermis. Anatomical studies have suggested that the ChAT+ MFs
482 located in lobules IX/X and the flocculus originate from medial vestibular nucleus (MVN) and
483 nucleus prepositus hypoglossi (NPH) (Barmack et al., 1992b), whereas ChAT+ beaded fibers
484 may originate from the pedunculopontine tegmental nuclei (PPTg) (Newman and Ginsberg, 1992;
485 Ruggiero et al., 1997; Woolf and Butcher, 1989). Notably, for any of these sources it remains
486 possible that other neurotransmitters are co-released with ACh as has been shown in other brain
487 regions (Granger et al., 2017). However, based on our goal of measuring the longer timescale

488 effects of ACh, we did not investigate the possibility of other fast transmitters that may also play
489 a role during the initial phases of transient ACh release.

490 Such diversity of sources of ACh suggests multiple roles for cholinergic signaling. Inputs
491 from the medial vestibular nucleus may be important for modulation of vestibular guided reflexes.
492 In support of a role for ACh in modulating vestibular guided behaviors, previous work has shown
493 that cerebellar injection of cholinergic agonists can enhance both OKR and VOR reflexes (Prestori
494 et al., 2013; Tan and Collewijn, 1991, 1992). Such findings are in line with an enhancement of
495 responses in granule cells, and particularly those receiving vestibular input. Thus, the increased
496 spike probabilities observed here in a subpopulation of granule cells may explain these previously
497 observed behavioral effects of ACh.

498 The presence of cholinergic inputs from the PPTg also suggest a role for ACh in contextual
499 modulation of the granule cell layer, for instance by arousal or locomotion. Indeed, recent work
500 has demonstrated a locomotion-dependent enhancement of learning in a cerebellar dependent
501 form of delay eyeblink conditioning (EBC) (Albergaria et al., 2018). Specifically, the acquisition
502 rate of delay EBC was correlated with the animals running speed. In this study, the circuit
503 mechanism underlying this enhancement was linked to an increase in granule cell layer
504 excitability (Albergaria et al., 2018). In this model, behaviorally relevant sensory information would
505 more easily drive granule cells past spike threshold during locomotion, and thus transmit more
506 effectively to downstream Purkinje cells to promote synaptic plasticity and learning. While
507 speculative, our results suggest the possibility that ACh could provide an endogenous mechanism
508 to disinhibit populations of granule cells and enable such locomotion-dependent effects on
509 learning. In particular, because the PPTg is active during locomotion (Lee et al., 2014), it could
510 provide the type of tonic acetylcholine release that would enhance granule cell responses and
511 promote associative learning. At present, however, it is unknown whether ACh is released into
512 the cerebellar cortex during locomotion.

513 Finally, our results suggest that the key determinant of how ACh modulates granule cell
514 spike probability is the initial balance of excitation and inhibition onto each cell. Indeed, previous
515 work has demonstrated that inhibition is not homogenous across granule cells (Crowley et al.,
516 2009). Such diversity may arise from a combination of factors, including differences in the number
517 of Golgi cell inputs per glomerulus (Jakab and Hamori, 1988), the number of granule cell dendrites
518 per cell (Palay and Chan-Palay, 1974), a diversity of Golgi cell types (Geurts et al., 2001; Neki et
519 al., 1996; Simat et al., 2007), or differences in GABA receptor expression at granule cell synapses
520 (Wall, 2002). Likewise, the amplitude of unitary excitatory mossy fiber conductances onto granule
521 cells has been shown to vary over a wide range, and depend on the source of the mossy fiber
522 input (Chabrol et al., 2015). Moreover, because granule cells can integrate multiple mossy fiber
523 inputs from diverse sources (Huang et al., 2013), it is possible for individual cells to exhibit
524 considerable variability in both the amount of excitation and inhibition they receive across the
525 population.

526 Notably, we find ACh selectively increases the excitability of the granule cells that are
527 most strongly inhibited. Previous work has suggested that that granule cell inhibition can be
528 stimulus-specific (Precht and Llinas, 1969), and recent work has indicated that such stimulus
529 specific inhibition may play a key role in cerebellar learning (Kalmbach et al., 2011). If different
530 Golgi cells can indeed be recruited by some stimuli and not others, cholinergic neuromodulation
531 would provide an ideal mechanism to enhance the responses of granule cells that would
532 otherwise be suppressed by stimulus-specific inhibition. Hence, such a mechanism could serve
533 to enhance learning for specific mossy fiber inputs, perhaps based on behavioral context or
534 stimulus salience. Thus, ACh neuromodulation would provide an appealing means to regulate
535 learning or modify the gain of cerebellar transformations. While future *in vivo* experiments will be
536 necessary to evaluate this possibility, our results reveal both the cell autonomous and circuit level
537 actions by which ongoing ACh release can act through muscarinic receptors to modulate granule

538 cell excitability. Such data thus provide the foundation for interpreting the *in vivo* effects of
539 cholinergic neuromodulation at the input stage of cerebellar processing.
540
541 **Figure Legends**
542
543 **Figure 1. Acetylcholine activates nicotinic and muscarinic (M2) receptors in Golgi cells but**
544 **does not act on granule cells. A)** Schematic showing intracellular recording of Golgi cells during
545 focal application of acetylcholine chloride (ACh). A glass pipette containing 500 μM ACh was
546 placed in close proximity to the soma. **B)** Representative current-clamp recording of spontaneous
547 activity in the presence of glutamatergic (NBQX 5 μM, CPP 2.5 μM) and GABAergic (SR-95531
548 5 μM) antagonist. A 200 ms pulse of ACh evokes a transient increase in spontaneous activity
549 followed by a pause. **C-D)** Normalized spike rate across stimulus presentations (normalized to
550 the 5 sec period prior to ACh stimulus, 1 sec bins, n = 10). **C)** Time course of ACh mediated
551 change in spike rate (group average). **D)** Average spike rate by cell (grey), group average (black,
552 mean ± SEM; ANOVA, $F_{1.052, 9.471} = 9.679$, P = 0.0111, n = 10) at 4 sec (0.99 ± 0.09 norm), 6 sec
553 (4.0 ± 1.1 norm, P = 0.0517), 10 sec (0.1 ± 0.06 norm, P = 0.0004), and 20 sec (1.1 ± 0.2 norm,
554 P = 0.9658). **E)** Voltage-clamp recordings from the same cell in B. A 200 ms pulse of ACh evokes
555 an outward current that is blocked by a selective muscarinic M2 antagonist (AF-DX116 1 μM),
556 and an inward current that is blocked by a non-selective nicotinic antagonist (MMA 10 μM). **F)**
557 Peak amplitudes from voltage-clamp recordings at -60 mV. Amplitudes were determined using
558 the subtracted average current for each cell (nicotinic: 40.3 ± 11.4 pA, muscarinic: 16.1 ± 2.6 pA,
559 n = 7). **G)** Schematic showing intracellular recording of granule cells during focal application of
560 acetylcholine chloride (ACh). A glass pipette containing 500 μM ACh was placed in close proximity
561 to the soma. **H)** Representative current clamp trace from a granule cell in the presence of
562 glutamatergic (NBQX 5 μM, CPP 2.5 μM) and GABAergic (SR-95531 5 μM) antagonist. A 500 ms

563 pulse of ACh fails to evoke change in the membrane potential. **I)** Average spike rate across all
564 cells (n = 24). **J)** Grouped voltage-clamp trace from all cells (n = 24).
565
566 **Figure 2. Activation of Muscarinic Receptors on Golgi Cells Hyperpolarizes the Membrane**
567 **A)** Whole cell current-clamp recordings from Golgi cell in the in the presence of a Na^+ channel
568 antagonist, tetrodotoxin (TTX, 0.5 μM), to block spontaneous firing. Bath application of muscarine
569 hyperpolarizes the membrane potential (musc: -65.2 ± 3.57 mV, n=6). **B-C)** Expression of
570 chronos-TdTomato in ChAT+ cerebellar projections. **C)** Expanded view of the cerebellar cortex
571 from B). Open arrows indicate thin, beaded fibers, closed arrow indicates mossy fiber-like
572 projection. **D)** Average voltage-clamp recording from an example Golgi cell (Vm = -55 mV) in
573 response to optogenetic stimulation (450 nm, 50 Hz, 15 mW, 2 sec) in control (black) and following
574 atropine application (5 μM, gray) (control average = 31.4 ± 4.8 pA, atropine average = 10.2 ± 2.3
575 pA, n = 8, p = 0.002, paired t-test). **E)** Summary of Golgi cell optogenetic stimulation experiments.
576
577 **Figure 3. Activation of muscarinic M2 receptors on Golgi cell decreases phasic and tonic**
578 **inhibition in granule cells. A)** Example whole-cell voltage clamp recording from a granule cell
579 held at the reversal potential of excitation (~10 mV) to record $GABA_A$ receptor-mediated phasic
580 and tonic inhibition (measured using sIPSC frequency and holding current, respectively). Dashed
581 horizontal line indicates no holding current. **B)** Grouped average spontaneous IPSC frequency
582 across time in the presence of muscarine (musc, 10 μM), atropine (5 μM), and $GABA_A$ antagonist
583 (SR-95531 5 μM; mean ± SEM, n = 11). **C)** Grouped average holding current across time. **D)** *Left*,
584 Summary of the change in sIPSC frequency for individual cells. Quantified using a 2-minute
585 window (control: 2-4', muscarine: 7-9', atropine: 12-14', values normalized to control; ANOVA,
586 $F_{1.041, 10.41}$=29.49, P = 0.0002, n = 11). Group average for each condition: muscarine (0.2 ± 0.0
587 norm, P<0.0001); atropine (1.2 ± 0.2 norm, P = 0.3773). *Right*, Summary of the change in holding
588 current (ANOVA, $F_{1.565, 15.65}$= 65.96, P<0.0001) for individual cells in muscarine (group average:

589 0.5 ± 0.0 norm, P<0.0001) and atropine (group average: 0.9 ± 0.1 norm, P = 0.0681). sIPSC and
590 tonic inhibition was confirmed using the $GABA_A$ antagonist (SR95531 5 μM).
591
592 **Figure 4. Activation of M2 receptors on Golgi cells invokes firing rate potentiation.** Whole-
593 cell, current-clamp recordings from Golgi cells before and during bath application of muscarine
594 (musc, 10 μM). **A)** *Top*, representative current-clamp recording during muscarine application.
595 Bath application of muscarine silences the spontaneous firing activity and this effect is reversed
596 by the non-selective mAChR antagonist, atropine. *Bottom*, normalized spike rate across all
597 experiments (rate at 5': 4.2 ± 0.6 Hz; 20': 5.5 ± 0.7 Hz; mean ± SEM; n = 17). **B)** Normalized spike
598 rate across experiments that had a baseline firing rate below 5 Hz (rate at 5': 3.2 ± 0.3 Hz; 20':
599 4.7 ± 0.6 Hz; n = 13). **C)** Normalized spike rate across experiments that had a baseline firing rate
600 above 5 Hz (rate at 5': 7.7 ± 1.5 Hz; 20': 7.9 ± 1.8 Hz; n = 4). **D)** Plot showing the initial spike rate
601 and FRP rate for individual cells. The degree of FRP was dependent on initial spike rate.
602
603 **Figure 5. Reduction of feed-forward inhibition by muscarinic receptors.**
604 **A)** Schematic showing the intracellular recording configuration and stimulus location, ~500–1000
605 μm from the cell. **B)** Representative voltage-clamp recordings of IPSCs (averaged from 30
606 consecutive events recorded at ~10 mV) evoked by electrical stimulation (2 pulses at 25 Hz, 100
607 μs pulse width) of mossy fibers in control, muscarine (10 μM), and atropine (5 μM). **C)** Response
608 patterns of evoked IPSCs (peak amplitude) for 30 consecutive trials in each drug condition.
609 Failures are shown in white. **D-E)** Summary of all recorded cells. **D)** Average amplitude of the first
610 evoked IPSC (30 consecutive trials, measurement includes successes and failures, values
611 normalized to control) in muscarine (10 μM, 0.0 ± 0.0 norm, P<0.0001), and atropine (5 μM, 1.1
612 ± 0.2 norm, P = 0.7283). Individual cells are depicted in grey, black lines and error bars show
613 mean ± SEM (ANOVA, $F_{1.003, 4.014}$ = 44.17, P = 0.0026, n = 5). **E)** Summary of IPSC failure rate to
614 the first stimulus in control (12.0 ± 5.83 %), muscarine (10 μM, 98.0 ± 0.8 %, P = 0.0004), and

615 atropine (5 μM, 19.3 ± 7.1 %, P = 0.4479), and glutamate antagonist (NQBX 5 μM & CPP 2.5 μM,
616 100.0 ± 0.0 %, P = 0.0003; ANOVA, $F_{1.561, 6.244}$ = 132.8, P<0.0001).
617
618 **Figure 6**. **Activation of presynaptic muscarinic receptors alters glutamatergic transmission**
619 **at the mossy fiber-Golgi cell synapse**. **A)** Schematic showing the intracellular recording
620 configuration and stimulus location. **B)** Representative voltage-clamp recordings of EPSCs
621 (averaged from 30 consecutive events recorded at -60 mV) evoked by electrical stimulation (2
622 pulses at 25 Hz, 100 μs pulse width) of mossy fibers in control, muscarine (10 μM), and atropine
623 (5 μM). **C)** Response patterns of evoked EPSCs (peak amplitude) for 30 consecutive trials in each
624 drug condition. Failures are shown in white. **D-G)** Summary of all recorded cells. **D)** Average
625 amplitude of the first evoked EPSC (30 consecutive trials, measurement includes successes and
626 failures, values normalized to control) in muscarine (10 μM, 0.4 ± 0.1 norm, P = 0.0035), and
627 atropine (5 μM, 0.9 ± 0.0 norm, P = 0.0439). Individual cells are depicted in grey, black lines and
628 error bars show mean ± SEM (ANOVA, $F_{1.192, 10.73}$=13.58, P = 0.0028, n = 10). **E)** Summary of
629 EPSC failure rate to the first stimulus in control (2.2 ± 0.96 %), muscarine (29.6 ± 8.52 %, P =
630 0.0358), atropine (2.2 ± 0.6 %, P = 0.8209), and glutamate antagonist (NQBX 5 μM & CPP 2.5
631 μM, 100.0 ± 0.0 %, P<0.0001; ANOVA, $F_{1.063, 9.565}$ = 120.9, P<0.0001, n = 10). **F)** Summary of
632 EPSC potency to the first stimulus (measurement excludes event failures) in control (1.0 ± 0.0
633 norm), muscarine (0.6 ± 0.1 norm, P = 0.0027), and atropine (0.9 ± 0.0 norm, P = 0.0792; ANOVA,
634 $F_{1.345, 12.11}$=13.72, P = 0.0017). **G)** Summary of paired-pulse ratio (PPR) in control (1.0 ± 0.1),
635 muscarine (1.0 ± 0.1 norm, P = 0.9895), and atropine (0.8 ± 0.1 norm, P = 0.5238; ANOVA, $F_{1.914,}$
636 $_{17.23}$=0.7338, P = 0.4889). **H)** Summary of paired-pulse ratio (PPR) in the presence of CGP (1
637 μM) in control (0.9 ± 0.0), muscarine (1.0 ± 0.1 norm, P = 0.7094), and atropine (0.8 ± 0.1 norm,
638 P = 0.3975; ANOVA, $F_{1.492, 13.43}$=1.225, P = 0.3040).
639
640

641 **Figure 7. Activation of presynaptic muscarinic receptors reduces glutamatergic**
642 **transmission at the mossy fiber-granule cell synapse**. **A)** Schematic showing the intracellular
643 recording configuration and stimulus location. **B)** Representative voltage-clamp recordings of
644 EPSCs (averaged from 30 consecutive events recorded at -70 mV) evoked by electrical
645 stimulation (2 pulses at 25 Hz, 100 μs pulse width) of mossy fibers in control, muscarine (10 μM),
646 and atropine (5 μM). **C)** Response patterns of evoked EPSCs (peak amplitude) for 30 consecutive
647 trials in each drug condition. Failures are shown in white. **D-G)** Summary of all recorded cells. **D)**
648 Average amplitude of the first evoked EPSC (30 consecutive trials, measurement includes
649 successes and failures, values normalized to control) in muscarine (10 μM, 0.5 ± 0.1 norm, P =
650 0.0007), and atropine (5 μM, 1.0 ± 0.1 norm, P = 0.8771). Individual cells are depicted in grey,
651 black lines and error bars show mean ± SEM (ANOVA, $F_{1.65, 14.85}$=14.98, P = 0.0005, n = 10). **E)**
652 Summary of EPSC failure rate to the first stimulus in control (0.3 ± 0.3 %), muscarine (10 μM,
653 26.3 ± 7.5 %, P = 0.017), and atropine (5 μM, 1.3 ± 0.7 %, P = 0.4037), and glutamate antagonist
654 (NQBX 5 μM & CPP 2.5 μM, 100.0 ± 0.00 %, P<0.0001; ANOVA, $F_{1.017, 9.156}$ = 160.0, P<0.0001).
655 **F)** Summary of EPSC potency to the first stimulus (measurement excludes event failures) in
656 control, muscarine (0.6 ± 0.1 norm, P = 0.0007), and atropine (1.0 ± 0.1 norm, P = 0.9183;
657 ANOVA, $F_{1.388, 12.49}$=10.02, P = 0.0047). **G)** Summary of paired-pulse ratio (PPR) in control (0.8 ±
658 0.0), muscarine (0.9 ± 0.1 norm, P = 0.8560), and atropine (0.8 ± 0.0 norm, P = 0.9951; ANOVA,
659 $F_{1.276, 11.49}$=0.2322, P = 0.6969).
660
661
662 **Figure 8. Muscarinic receptors modulate GrC spike probability. A)** Schematic showing the
663 cell-attached recording configuration and stimulus location. **B)** Representative cell-attached
664 recording. Stimulus intensity was set to generate GrC spiking with approximately 20-60 %
665 probability in response to either the 2nd or 3rd stimulus (3 pulses at 40Hz, repeated at 0.1 Hz). **C)**
666 Spike raster from an example granule cell that increased spike probability in muscarine. **D)**

667 Summary of spike probability across all granule cells that increased spiking in muscarine (n=5).
668 Spike probability was measured by normalizing each cell to its maximum response in control. **E)**
669 Spike raster from an example granule cell that decreased spike probability in muscarine. **F)**
670 Summary of spike probability across all granule cells that decreased spiking in muscarine (n=3).
671 **G)** Summary of spike rates in control, muscarine (10 μM, 1.2 ± 0.4 norm, P = 0.9087), atropine (5
672 μM, 0.9 ± 0.2 norm, P = 0.8923), $GABA_A$ antagonist (GABAzine, 5 μM, 6.8 ± 1.6 norm, P = 0.0259),
673 and glutamatergic antagonists (NQBX 5 μM & CPP 2.5 μM, 0.3 ± 0.1 norm, P = 0.0021; ANOVA,
674 $F_{1.076, 7.53}$ = 14.95, P = 0.0049, n = 8). **H)** Summary of the first spike latency in each drug condition
675 (mean & SD). Grouped average to 1st stimulus (3.8 ± 0.2 ms), 2nd (2.4 ± 0.1 ms), and 3rd (2.6 ±
676 0.1 ms; two-way ANOVA, $F_{3, 84}$ = 1.01, P = 0.3925).
677
678 **Figure 9**. A computational model shows that the heterogeneity in granule cell responses can be
679 explained by the variability in input connectivity and synaptic conductances. **A)** Summary of spike
680 probability across all simulated granule cells that increased spiking in muscarine. **B)** Summary of
681 spike probability across all simulated granule cells that decreased spiking in muscarine. **C)**
682 Summary of peak spike probabilities for simulated granule cells from (A) and (B) in muscarine vs.
683 control. Black denotes granule cells that increased spike probability, and gray denotes cells that
684 decreased spike probability. **D)** Summary of granule cell peak spike probability in muscarine vs.
685 number of active mossy fiber inputs. **E)** Summary of granule cell peak spike probability in
686 muscarine vs. average net (excitatory – inhibitory) conductance in control conditions. **F)** Granule
687 cell peak spike probability in muscarine vs. fractional reduction of inhibitory tonic current. **G)**
688 Summary of the average net control conductance (left) and inhibitory tonic current (right) for
689 simulated granule cells that increased (black) or decreased (gray) spiking in muscarine. **H)**
690 Distributions of average net input in control for simulated granule cells that increased (black) or
691 decreased (gray) spiking in muscarine. **I)** Distributions of fractional reduction of inhibitory tonic
692 current in simulated granule cells that increased (black) or decreased (gray) spiking in muscarine.

693 **References**

694

695 Albergaria, C., Silva, N.T., Pritchett, D.L., and Carey, M.R. (2018). Locomotor activity modulates
696 associative learning in mouse cerebellum. Nature Neuroscience 21, 725-735.

697 Albus, J.S. (1971). A theory of cerebellar function. Mathematical Biosciences 10, 25-61.

698 Barmack, N.H., Baughman, R.W., and Eckenstein, F.P. (1992a). Cholinergic innervation of the
699 cerebellum of rat, rabbit, cat, and monkey as revealed by choline acetyltransferase activity and
700 immunohistochemistry. The Journal of comparative neurology 317, 233-249.

701 Barmack, N.H., Baughman, R.W., Eckenstein, F.P., and Shojaku, H. (1992b). Secondary
702 vestibular cholinergic projection to the cerebellum of rabbit and rat as revealed by choline
703 acetyltransferase immunohistochemistry, retrograde and orthograde tracers. The Journal of
704 comparative neurology 317, 250-270.

705 Brickley, S.G., Cull-Candy, S.G., and Farrant, M. (1996). Development of a tonic form of
706 synaptic inhibition in rat cerebellar granule cells resulting from persistent activation of GABAA
707 receptors. The Journal of Physiology 497 (Pt 3), 753-759.

708 Cayco-Gajic, A., Clopath, C., and Silver, R.A. (2017). Sparse synaptic connectivity is required
709 for decorrelation and pattern separation in feedforward networks. Nature Communications 8.

710 Chabrol, F.P., Arenz, A., Wiechert, M.T., Margrie, T.W., and DiGregorio, D.A. (2015). Synaptic
711 diversity enables temporal coding of coincident multisensory inputs in single neurons. Nature
712 Neuroscience.

713 Crowley, J.J., Fioravante, D., and Regehr, W.G. (2009). Dynamics of Fast and Slow Inhibition
714 from Cerebellar Golgi Cells Allow Flexible Control of Synaptic Integration. Neuron 63, 843-853.

715 Didier, M., Berman, S.A., Lindstrom, J., and Bursztajn, S. (1995). Characterization of nicotinic
716 acetylcholine receptors expressed in primary cultures of cerebellar granule cells. Molecular
717 Brain Research 30, 17-28.

718 Dominguez de Toro, E., Juíz, J.M., Smillie, F.I., Lindstrom, J., and Criado, M. (1997).
719 Expression of α 7 neuronal nicotinic receptors during postnatal development of the rat
720 cerebellum. Developmental Brain Research 98, 125-133.

721 Dominguez del Toro, E., Juiz, J.M., Peng, X., Lindstrom, J., and Criado, M. (1994).
722 Immunocytochemical localization of the alpha 7 subunit of the nicotinic acetylcholine receptor in
723 the rat central nervous system. The Journal of comparative neurology 349, 325-342.

724 Duguid, I., Branco, T., Chadderton, P., Arlt, C., Powell, K., and Häusser, M. (2015). Control of
725 cerebellar granule cell output by sensory-evoked Golgi cell inhibition. Proceedings of the
726 National Academy of Sciences of the United States of America 112, 13099-13104.

727 Duguid, I., Branco, T., London, M., Chadderton, P., and Hausser, M. (2012). Tonic Inhibition
728 Enhances Fidelity of Sensory Information Transmission in the Cerebellar Cortex. Journal of
729 Neuroscience 32, 11132-11143.

730 Eccles, J., Llinás, R., and Sasaki, K. (1966). The mossy fibre-granule cell relay of the
731 cerebellum and its inhibitory control by Golgi cells. Experimental Brain Research.

732 Farrant, M., and Brickley, S.G. (2003). Properties of GABAA receptor-mediated transmission at
733 newly formed Golgi-granule cell synapses in the cerebellum. Neuropharmacology 44, 181-189.

734 Fleming, E., and Hull, C. (2019). Serotonin regulates dynamics of cerebellar granule cell activity
735 by modulating tonic inhibition. J Neurophysiol 121, 105-114.

736 Forti, L., Cesana, E., Mapelli, J., and D'Angelo, E. (2006). Ionic mechanisms of
737 autorhythmic firing in rat cerebellar Golgi cells. The Journal of Physiology 574, 711-729.

738 Froemke, R.C., Carcea, I., Barker, A.J., Yuan, K., Seybold, B.A., Martins, A.R.O., Zaika, N.,
739 Bernstein, H., Wachs, M., Levis, P.A.*, et al.* (2013). Long-term modification of cortical synapses
740 improves sensory perception. Nature Neuroscience 16, 79-88.

741 Geurts, F.J., Timmermans, J., Shigemoto, R., and De Schutter, E. (2001). Morphological and
742 neurochemical differentiation of large granular layer interneurons in the adult rat cerebellum.
743 Neuroscience 104, 499-512.

744 Gilmer, J.I., and Person, A.L. (2017). Morphological Constraints on Cerebellar Granule Cell
745 Combinatorial Diversity. The Journal of neuroscience : the official journal of the Society for
746 Neuroscience 37, 12153-12166.

747 Giovannucci, A., Badura, A., Deverett, B., Najafi, F., Pereira, T.D., Gao, Z., Ozden, I., Kloth,
748 A.D., Pnevmatikakis, E., Paninski, L.*, et al.* (2017). Cerebellar granule cells acquire a
749 widespread predictive feedback signal during motor learning. Nature Neuroscience 20, 727-734.

750 Granger, A.J., Wallace, M.L., and Sabatini, B.L. (2017). Multi-transmitter neurons in the
751 mammalian central nervous system. Curr Opin Neurobiol 45, 85-91.

752 Huang, C.C., Sugino, K., Shima, Y., Guo, C., Bai, S., Mensh, B.D., Nelson, S.B., and Hantman,
753 A.W. (2013). Convergence of pontine and proprioceptive streams onto multimodal cerebellar
754 granule cells. Elife 2, e00400.

755 Hull, C.A., Chu, Y., Thanawala, M., and Regehr, W.G. (2013). Hyperpolarization Induces a
756 Long-Term Increase in the Spontaneous Firing Rate of Cerebellar Golgi Cells. Journal of
757 Neuroscience 33, 5895-5902.

758 Ito, M. (2006). Cerebellar circuitry as a neuronal machine. Progress in Neurobiology 78, 272-
759 303.

760 Ito, M. (2012). The Cerebellum (FT Press).

761 Jaarsma, D., Diño, M.R., Cozzari, C., and Mugnaini, E. (1996). Cerebellar choline
762 acetyltransferase positive mossy fibres and their granule and unipolar brush cell targets: a
763 model for central cholinergic nicotinic neurotransmission. Journal of Neurocytology 25, 829-842.

764 Jaarsma, D., Ruigrok, T., Caffé, R., and Cozzari, C. (1997). Cholinergic innervation and
765 receptors in the cerebellum. Progress in brain.

766 Jakab, R.L., and Hamori, J. (1988). Quantitative morphology and synaptology of cerebellar
767 glomeruli in the rat. Anat Embryol (Berl) 179, 81-88.

768 Kalmbach, B.E., Voicu, H., Ohyama, T., and Mauk, M.D. (2011). A subtraction mechanism of
769 temporal coding in cerebellar cortex. J Neurosci 31, 2025-2034.

770 Kanichay, R.T., and Silver, R.A. (2008). Synaptic and Cellular Properties of the Feedforward
771 Inhibitory Circuit within the Input Layer of the Cerebellar Cortex. Journal of Neuroscience 28,
772 8955-8967.

773 Kuchibhotla, K.V., Gill, J.V., Lindsay, G.W., Papadoyannis, E.S., Field, R.E., Sten, T.A.H.,
774 Miller, K.D., and Froemke, R.C. (2017). Parallel processing by cortical inhibition enables
775 context-dependent behavior. Nature Neuroscience 20, 62-71.

776 Lee, A.M., Hoy, J.L., Bonci, A., Wilbrecht, L., Stryker, M.P., and Niell, C.M. (2014). Identification
777 of a brainstem circuit regulating visual cortical state in parallel with locomotion. Neuron 83, 455-
778 466.

779 Letzkus, J.J., Wolff, S.B.E., Meyer, E.M.M., Tovote, P., Courtin, J., Herry, C., and Lüthi, A.
780 (2011). A disinhibitory microcircuit for associative fear learning in the auditory cortex. Nature
781 480, 331-335.

782 Marr, D. (1969). A theory of cerebellar cortex. The Journal of Physiology.

783 Mauk, M.D., and Buonomano, D.V. (2004). The neural basis of temporal processing. Annual
784 Review of Neuroscience 27, 307-340.

785 Nakayama, H., Shioda, S., Nakajo, S., Ueno, S., Nakashima, T., and Nakai, Y. (1997).
786 Immunocytochemical localization of nicotinic acetylcholine receptor in the rat cerebellar cortex.
787 Neuroscience Research 29, 233-239.

788 Neki, a., Ohishi, H., Kaneko, T., Shigemoto, R., Nakanishi, S., and Mizuno, N. (1996).
789 Metabotropic glutamate receptors mGluR2 and mGluR5 are expressed in two non-overlapping
790 populations of Golgi cells in the rat cerebellum. Neuroscience 75, 815-826.

791 Neustadt, A., Frostholm, A., and Rotter, A. (1988). Topographical distribution of muscarinic
792 cholinergic receptors in the cerebellar cortex of the mouse, rat, guinea pig, and rabbit: A species
793 comparison. Journal of Comparative Neurology 272, 317-330.

794 Newman, D.B., and Ginsberg, C.Y. (1992). Brainstem Reticular Nuclei that Project to the
795 Cerebellum in Rats A Retrograde Tracer Study; pp. 24–38. Brain, Behavior and Evolution 39,
796 24-38.

797 Ojima, H., Kawajiri, S.I., and Yamasaki, T. (1989). Cholinergic innervation of the rat cerebellum:
798 Qualitative and quantitative analyses of elements immunoreactive to a monoclonal antibody
799 against choline acetyltransferase. Journal of Comparative Neurology 290, 41-52.

800 Ozden, I., Dombeck, D.A., Hoogland, T.M., Tank, D.W., and Wang, S.S.H. (2012). Widespread
801 State-Dependent Shifts in Cerebellar Activity in Locomoting Mice. PloS one 7, e42650.

802 Palay, S.L., and Chan-Palay, V. (1974). Cerebellar cortex (New York: Springer).

803 Precht, W., and Llinas, R. (1969). Functional organization of the vestibular afferents to the
804 cerebellar cortex of frog and cat. Exp Brain Res 9, 30-52.

805 Prestori, F., Bonardi, C., Mapelli, L., Lombardo, P., Goselink, R., De Stefano, M.E., Gandolfi, D.,
806 Mapelli, J., Bertrand, D., Schonewille, M.*, et al.* (2013). Gating of Long-Term Potentiation by
807 Nicotinic Acetylcholine Receptors at the Cerebellum Input Stage. PloS one 8, e64828.

808 Ruggiero, D.A., Anwar, M., Golanov, E.V., and Reis, D.J. (1997). The pedunculopontine
809 tegmental nucleus issues collaterals to the fastigial nucleus and rostral ventrolateral reticular
810 nucleus in the rat. Brain Research 760, 272-276.

811 Simat, M., Parpan, F., and Fritschy, J.-m. (2007). Heterogeneity of Glycinergic and Gabaergic
812 Interneurons in the Granule Cell Layer of Mouse Cerebellum. Comparative and General
813 Pharmacology 83, 71-83.

814 Solinas, S., Nieus, T., and D'Angelo, E. (2010). A realistic large-scale model of the cerebellum
815 granular layer predicts circuit spatio-temporal filtering properties. Front Cell Neurosci 4, 12.

816 Takayasu, Y., Iino, M., Furuya, N., and Ozawa, S. (2003). Muscarine-induced increase in
817 frequency of spontaneous EPSCs in Purkinje cells in the vestibulo-cerebellum of the rat. Journal
818 of Neuroscience 23, 6200-6208.

819 Tan, H.S., and Collewijn, H. (1991). Cholinergic modulation of optokinetic and vestibulo-ocular
820 responses: a study with microinjections in the flocculus of the rabbit. Experimental Brain
821 Research 85, 475-481.

822 Tan, H.S., and Collewijn, H. (1992). Cholinergic and noradrenergic stimulation in the rabbit
823 flocculus have synergistic facilitatory effects on optokinetic responses. Brain Research 586,
824 130-134.

825 Turner, J.R., and Kellar, K.J. (2005). Nicotinic cholinergic receptors in the rat cerebellum:
826 multiple heteromeric subtypes. Journal of Neuroscience 25, 9258-9265.

827 Wagner, M.J., Kim, T.H., Savall, J., Schnitzer, M.J., and Luo, L. (2017). Cerebellar granule cells
828 encode the expectation of reward. Nature Publishing Group 544, 1-18.

829 Wall, M.J. (2002). Furosemide reveals heterogeneous GABA(A) receptor expression at adult rat
830 Golgi cell to granule cell synapses. Neuropharmacology 43, 737-749.

831 Woolf, N.J., and Butcher, L.L. (1989). Cholinergic systems in the rat brain: IV. descending
832 projections of the pontomesencephalic tegmentum. Brain Research Bulletin 23, 519-540.

833 Yardeni, T., Eckhaus, M., Morris, H.D., Huizing, M., and Hoogstraten-Miller, S. (2011). Retro-
834 orbital injections in mice. Lab Anim (NY) 40, 155-160.

835

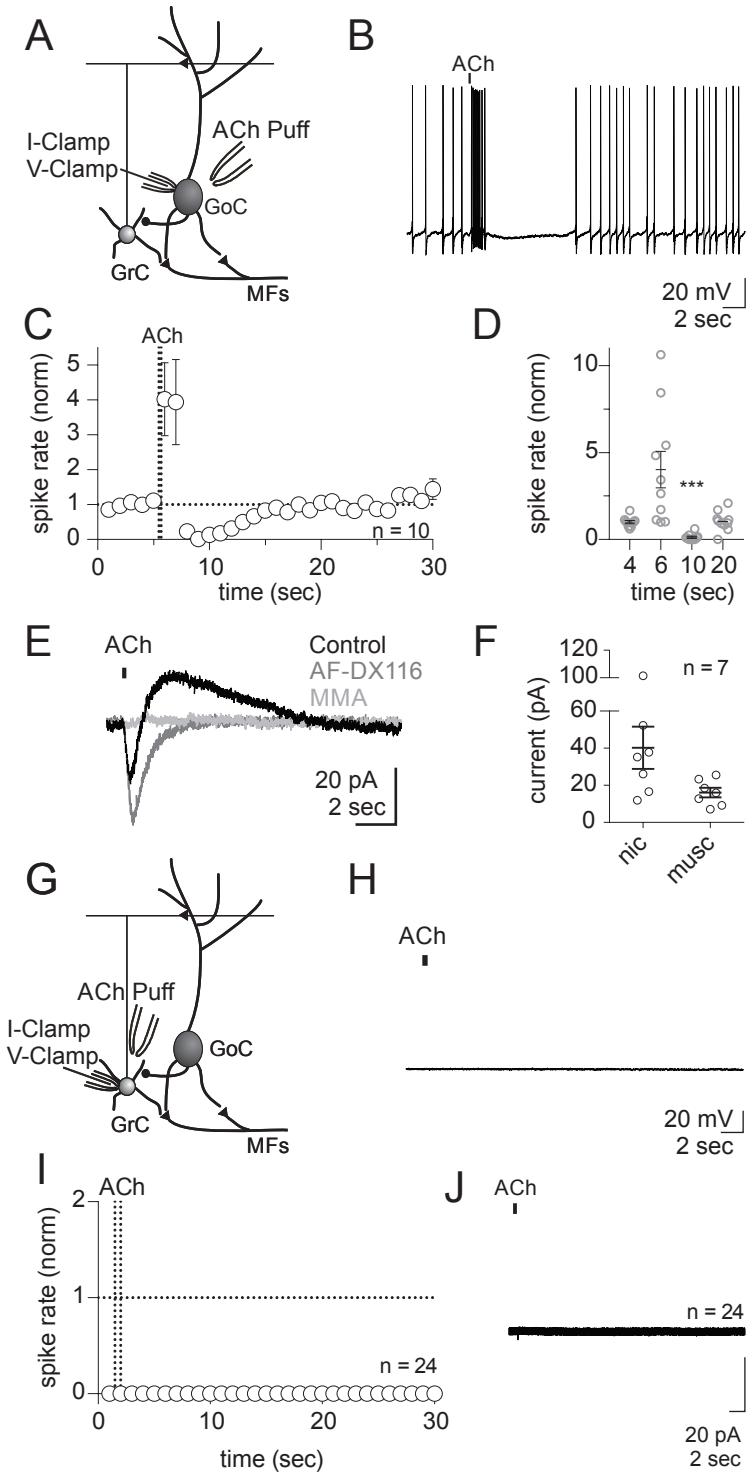
A
I-Clamp
V-Clamp
ACh Puff
GoC
GrC
MFs
B
ACh
20 mV
2 sec
C
ACh
spike rate (norm)
n = 10
time (sec)
D
spike rate (norm)
***
time (sec)
E
ACh
Control
AF-DX116
MMA
20 pA
2 sec
F
current (pA)
n = 7
nic
musc
G
ACh Puff
I-Clamp
V-Clamp
GoC
GrC
MFs
H
ACh
20 mV
2 sec
I
ACh
spike rate (norm)
n = 24
time (sec)
J
ACh
n = 24
20 pA
2 sec

Figure 1

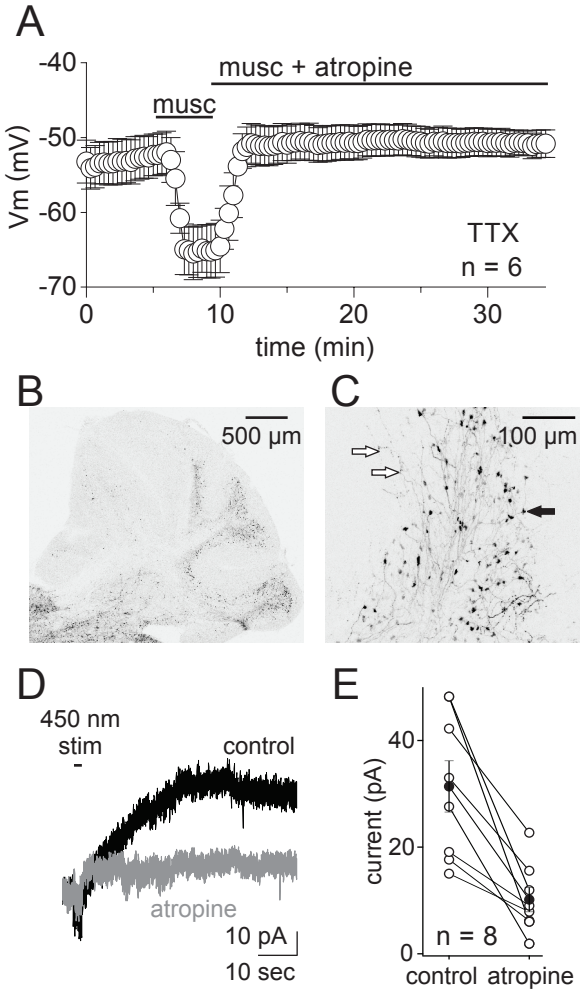
A
musc + atropine
musc
Vm (mV)
-40
-50
-60
-70
TTX
n = 6
0
10
20
30
time (min)
B
500 µm
C
100 µm
D
450 nm
stim
control
atropine
10 pA
10 sec
E
current (pA)
40
20
0
n = 8
control
atropine

Figure 2

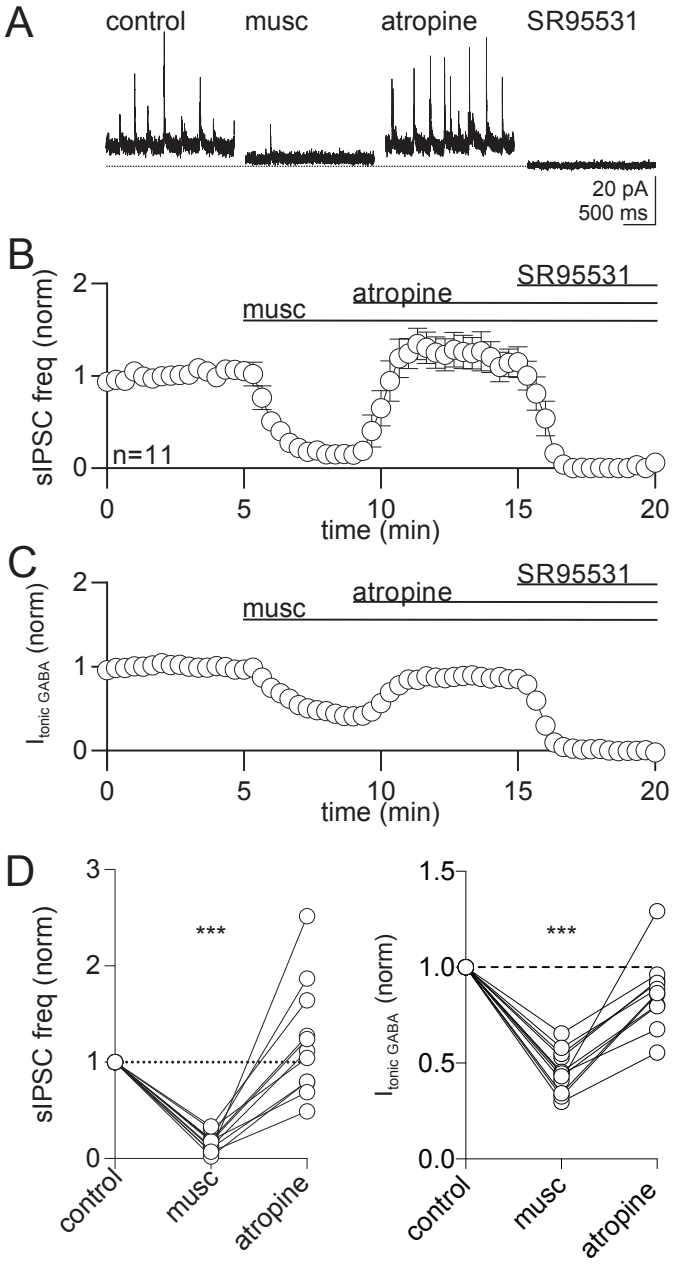
A
control
musc
atropine
SR95531
20 pA
500 ms
B
sIPSC freq (norm)
musc
atropine
SR95531
n=11
time (min)
C
$I_{tonic\ GABA}$ (norm)
musc
atropine
SR95531
time (min)
D
sIPSC freq (norm)
***
control
musc
atropine
$I_{tonic\ GABA}$ (norm)
***
control
musc
atropine

Figure 3

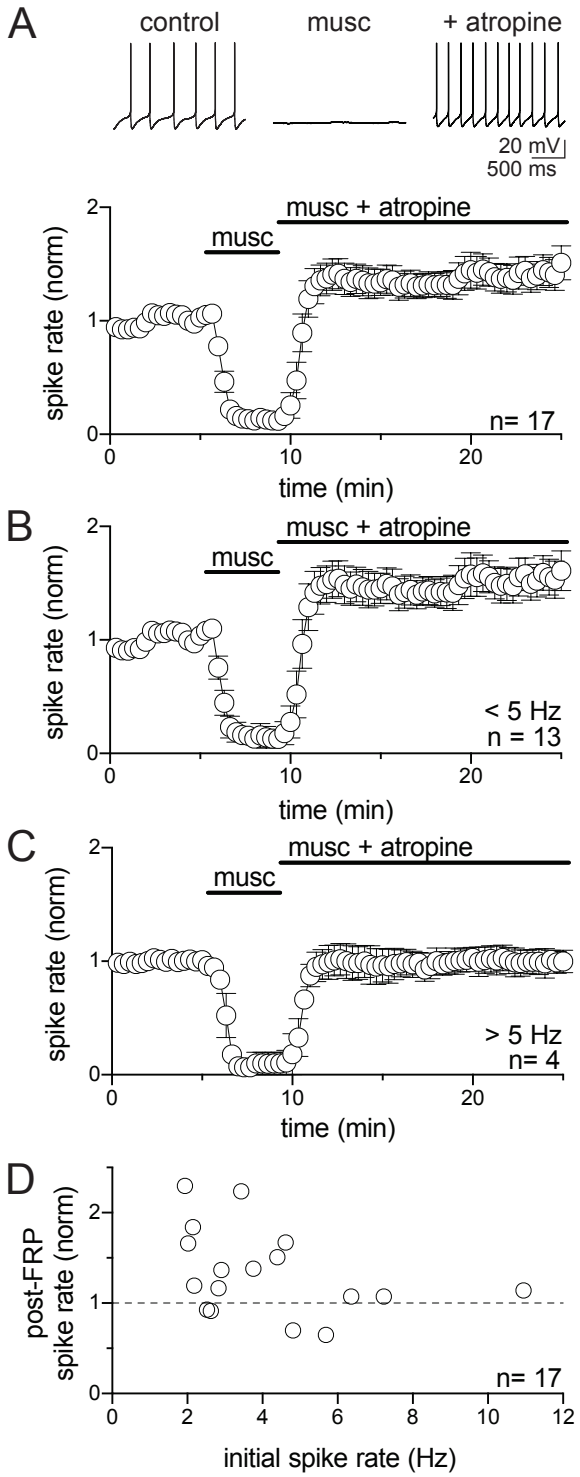
A
control
musc
+ atropine
20 mV
500 ms
musc + atropine
musc
spike rate (norm)
n= 17
time (min)
B
musc + atropine
musc
spike rate (norm)
< 5 Hz
n = 13
time (min)
C
musc + atropine
musc
spike rate (norm)
> 5 Hz
n= 4
time (min)
D
post-FRP
spike rate (norm)
n= 17
initial spike rate (Hz)

Figure 4

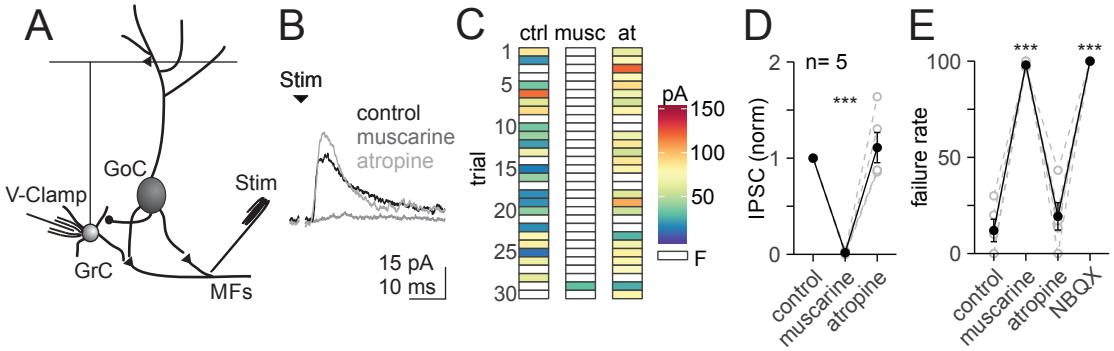
A
B
C
D
E
V-Clamp
GoC
GrC
Stim
MFs
Stim
control
muscarine
atropine
15 pA
10 ms
ctrl musc at
trial
pA
150
100
50
F
n= 5
IPSC (norm)
control
muscarine
atropine
failure rate
NBQX
***

Figure 5

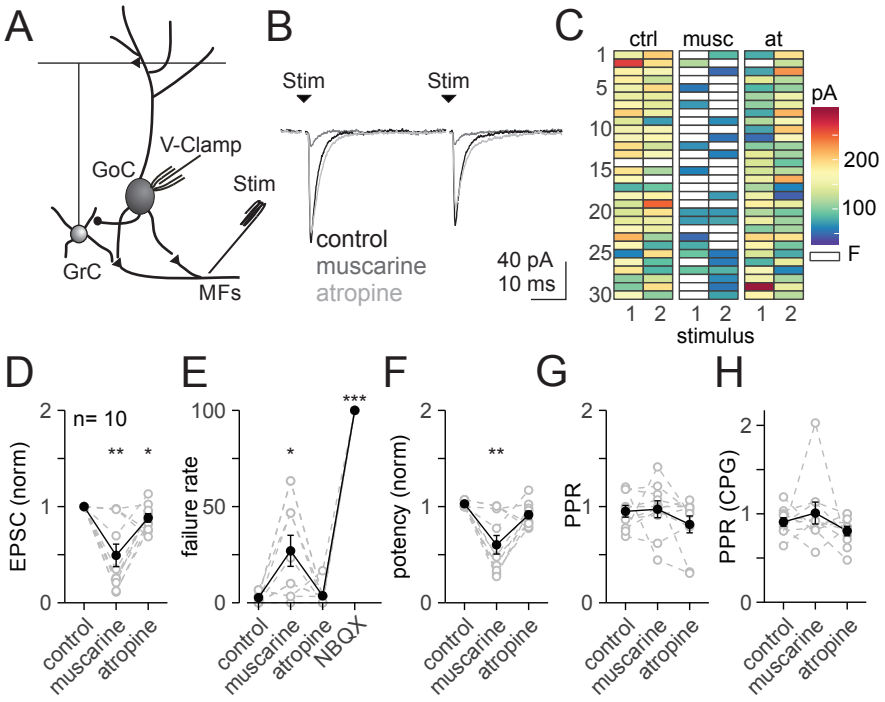
A
B
C
V-Clamp
GoC
Stim
GrC
MFs
Stim
Stim
control
muscarine
atropine
40 pA
10 ms
ctrl
musc
at
pA
200
100
F
stimulus
D
E
F
G
H
n= 10
EPSC (norm)
failure rate
potency (norm)
PPR
PPR (CPG)
control
muscarine
atropine
NBQX

Figure 6

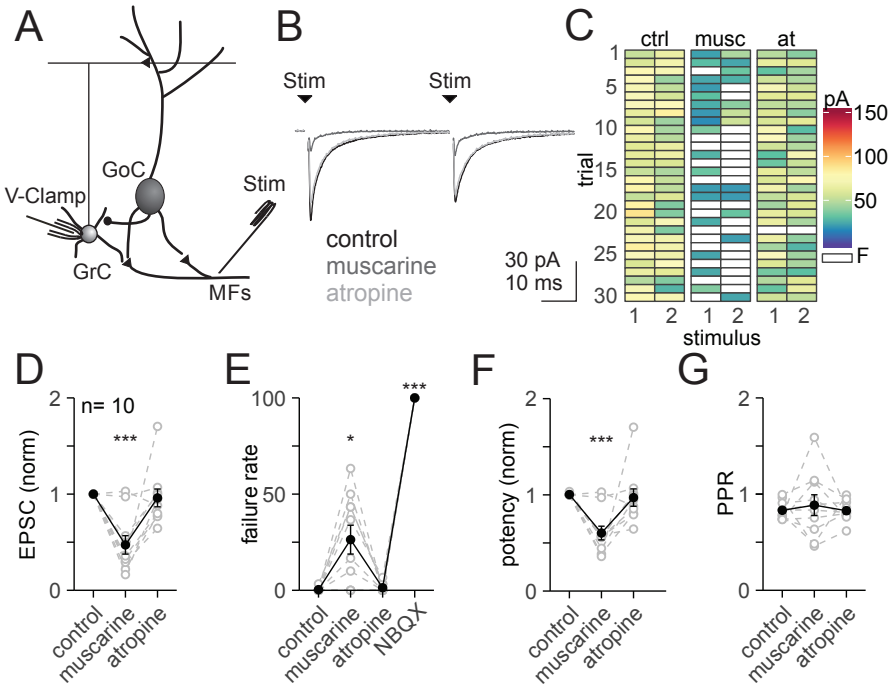
A
GoC
V-Clamp
Stim
GrC
MFs
B
Stim
Stim
control
muscarine
atropine
30 pA
10 ms
C
ctrl
musc
at
trial
pA
150
100
50
F
stimulus
D
n= 10
EPSC (norm)
control
muscarine
atropine
E
failure rate
NBQX
F
potency (norm)
G
PPR

Figure 7

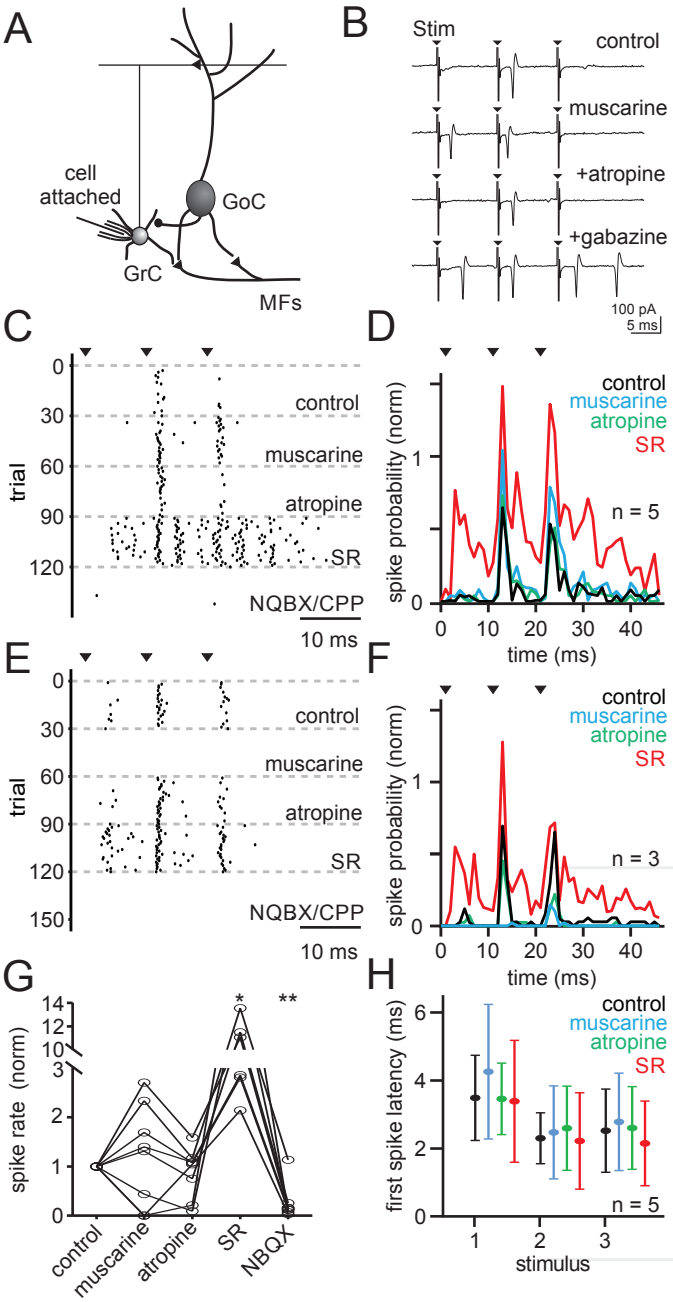
A
cell
attached
GoC
GrC
MFs
B
Stim
control
muscarine
+atropine
+gabazine
100 pA
5 ms
C
trial
control
muscarine
atropine
SR
NQBX/CPP
10 ms
D
spike probability (norm)
control
muscarine
atropine
SR
n = 5
time (ms)
E
trial
control
muscarine
atropine
SR
NQBX/CPP
10 ms
F
spike probability (norm)
control
muscarine
atropine
SR
n = 3
time (ms)
G
spike rate (norm)
control
muscarine
atropine
SR
NBQX
H
first spike latency (ms)
control
muscarine
atropine
SR
n = 5
stimulus

Figure 8

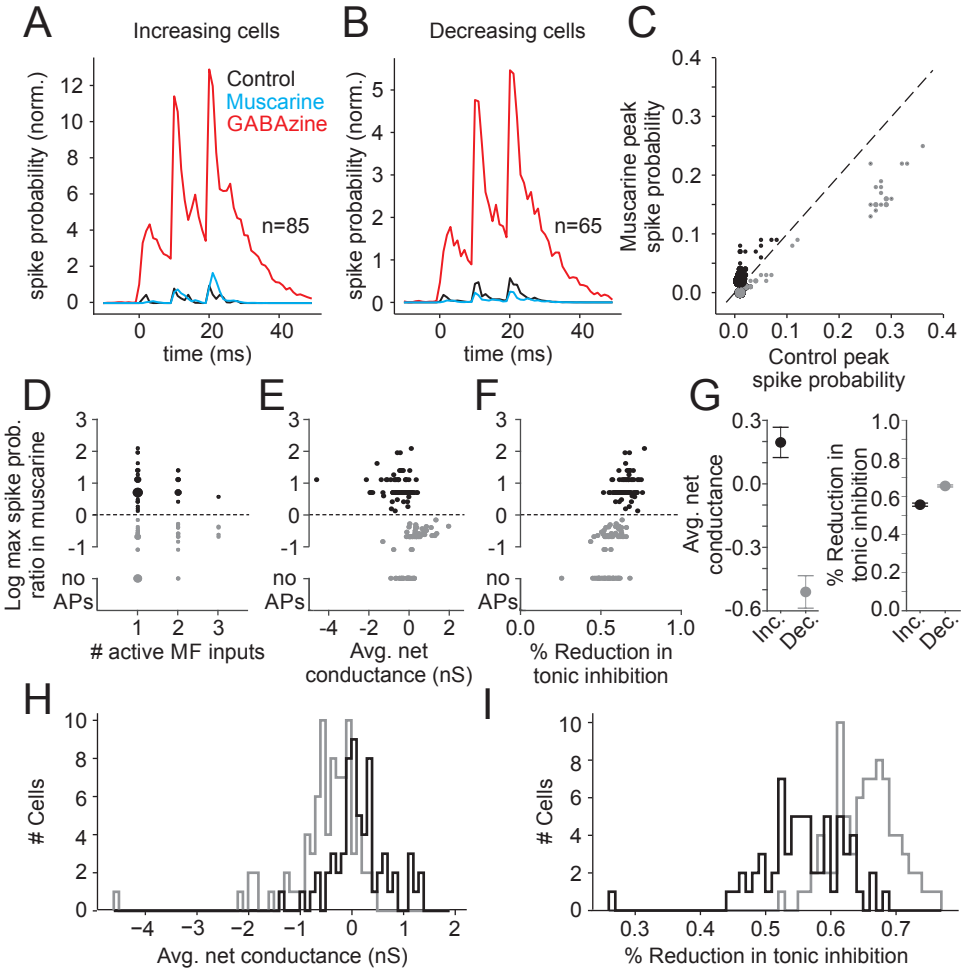
A
Increasing cells
Control
Muscarine
GABAzine
n=85
spike probability (norm.)
time (ms)
B
Decreasing cells
n=65
spike probability (norm.)
time (ms)
C
Muscarine peak spike probability
Control peak spike probability
D
Log max spike prob. ratio in muscarine
no APs
active MF inputs
E
Avg. net conductance (nS)
F
% Reduction in tonic inhibition
G
Avg. net conductance
% Reduction in tonic inhibition
Inc.
Dec.
H
Cells
Avg. net conductance (nS)
I
Cells
% Reduction in tonic inhibition

Figure 9